Int. J. Electrochem. Sci., 15 **(2020)** 8721 – 8731, doi: 10.20964/2020.09.68

International Journal of
ELECTROCHEMICAL
SCIENCE
www.electrochemsci.org

Fabrication of Cu_2O/rGO Hydrogel Film and its Application as Electrochemical Hydrogen Peroxide Sensor

Qishi Zhong, Zhiyong Zhao, Zhihua Liu, Yujun Qin[*]

Department of Chemistry, Renmin University of China, Beijing 100872, China
[*]E-mail: yjqin@ruc.edu.cn

Received: 8 March 2020 / *Accepted:* 19 May 2020 / *Published:* 10 August 2020

The exploration of graphene-based electrochemical sensors has aroused intensive interest in application research. Here, we report the decoration of a reduced graphene oxide hydrogel film with Cu_2O through a facile electrodeposition method and show that the as-prepared Cu_2O/graphene hydrogel film can be directly utilized as an electrochemical H_2O_2 sensor. The morphology and structure of the hydrogel composite are characterized, and the optimal electrodeposition time is determined. The graphene/Cu_2O hydrogel film acting as a H_2O_2 sensor exhibits high electrochemical sensing properties in terms of response, detection limit and selectivity. The present study could expand the potential of graphene hydrogel materials in the fields of sensors and biosensors.

Keywords: Graphene; Electrodeposition; Cuprous oxide; Hydrogen peroxide; Sensors.

1. INTRODUCTION

Owing to its exceptional structure and extraordinary properties [1], graphene has become the most promising material in many fields in recent years [2]. In particular, the advantages of high specific surface area, superior conductivity and chemical stability make graphene a good substrate to build electrochemical sensors and biosensors [3-5]. Therefore, the reliable detection of hydrogen peroxide (H_2O_2) is of the most significant potential owing to its indispensability in food analysis, environmental protection and enzymatic reactions [6-7]. Typically, traditional enzyme-based electrochemical sensors have shown good H_2O_2 detection performance, while their application is limited to some extent by their sensitivity to pH and temperature [8]. As a result, research interest in fabricating enzyme-free graphene-based sensors has recently increased, resulting in superior electrocatalytic performance in H_2O_2 reduction owing to the unique properties of graphene [9].

In general, the preparation of graphene-incorporated enzyme-free H_2O_2 sensors involves the decoration of graphene sheets with noble-metal nanoparticles [10], such as Au [11], Ag [12] and Pt [13].

For example, Yang *et al*. reported the preparation of graphene films embedded with Au nanoparticles through electrostatic assembly and thermal treatment, with high performance for electrochemical H_2O_2 sensing [14]. However, the application of noble metals may limit further development in practice. In addition, transition metal oxides have been adopted to prepare graphene-based electrochemical sensors [15], including Co_3O_4 [16], MnO_2 [17] and Cu_2O [18]. Among them, Cu_2O has been considered a promising candidate for fabricating biosensors, including H_2O_2 sensors, owing to its high catalytic activity and low cost [19]. Chen *et al.* synthesized a Cu_2O/graphene composite through a hydrothermal process to be used as a modifier of a glassy carbon electrode (GCE), achieving excellent H_2O_2 sensing performance [20]. However, the fabrication of such sensors usually involves complicated procedures for graphene/Cu_2O composite preparation, dispersion and GCE modification.

The electrodeposition method, with the advantages of convenience and controllability, has obtained increasing application in the preparation of hierarchical nanocarbon/inorganic oxide composites, for example, battery and supercapacitor electrodes [21]. The electrochemical deposition of reduced graphene oxide (rGO) and/or Cu_2O has also been realized in the fabrication of graphene/Cu_2O composites for transparent electrodes [22], hydrogen generation [23] and electrochemical sensors [24]. For instance, Kuila *et al.* reported the consecutive electrodeposition of graphene nanoplatelets and Cu_2O nanoparticles on a stainless steel sheet, from which the as-prepared Cu_2O-graphene composite showed good performance for the detection of H_2O_2 [25].

To date, the electrodeposition preparation of graphene/Cu_2O composites has mainly been carried out on conductive substrates, such as GCE, nickel foam and stainless steel. Han *et al.* directly applied graphene microfibers as working electrodes for Cu_2O electrodeposition, which subsequently act as H_2O_2 sensors without additional substrates [26]. In addition, graphene hydrogels, as important 3D-structured graphene materials [27], have shown excellent behavior as electrochemical capacitors [28]. Such porous hierarchical graphene materials have potential for use as electrode substrates for electrodeposition, upon which the resulting hydrogel composites could be utilized as electrochemical sensors.

Herein, we report a feasible method of fabricating a Cu_2O/rGO hydrogel film and demonstrate its application in H_2O_2 sensing. The rGO hydrogel was prepared under mild conditions, which avoided high temperature and pressure. Then, Cu_2O particles were attached to the rGO hydrogel piece by the electrodeposition method. The Cu_2O/rGO composite films were directly applied as electrode sensors, exhibiting satisfactory performance in detecting H_2O_2.

2. EXPERIMENTAL

Sodium acetate trihydrate ($NaAc{\cdot}3H_2O$), sodium citrate, copper acetate monohydrate ($Cu(Ac)_2{\cdot}H_2O$)) and ascorbic acid were supplied by Alfa-Aesar. Poly(vinyl pyrrolidone) (PVP, NW≈30,000) was purchased from Aladdin. H_2O_2 solution (30 wt%) and other chemicals were purchased from Beijing Reagent Factory. GO was synthesized according to a previously reported method [29]. To prepare the rGO hydrogel, 120 mg of ascorbic acid was mixed with 5 mL of aqueous GO solution (8.4 mg/mL) in a sample bottle under constant stirring. Then, $NH_3{\cdot}H_2O$ was added to adjust the pH to 10.5,

and the mixture was stirred for 15 min. Finally, the bottle was kept at 60 °C in a water bath overnight, and the obtained hydrogel was washed with deionized water/ethanol before being treated in a vacuum freeze-dryer (–50 °C).

The rGO film cut from the aerogel composite wrapped with copper adhesive was applied as the working electrode for the electrodeposition of Cu_2O in a standard three-electrode system in a solution of 0.1 M NaAc, 0.01 M sodium citrate, 0.02 M $Cu(Ac)_2$ and 4 mg/mL PVP [30]. Pt and Ag-AgCl electrodes were used as the counter and reference electrodes, respectively. Electrodeposition was performed at a potential of –0.20 V at room temperature for 2, 8 and 16 min, with the final products denoted as rGO/Cu_2O-2, rGO/Cu_2O-8 and rGO/Cu_2O-16, respectively. The entire process is outlined in Scheme 1.

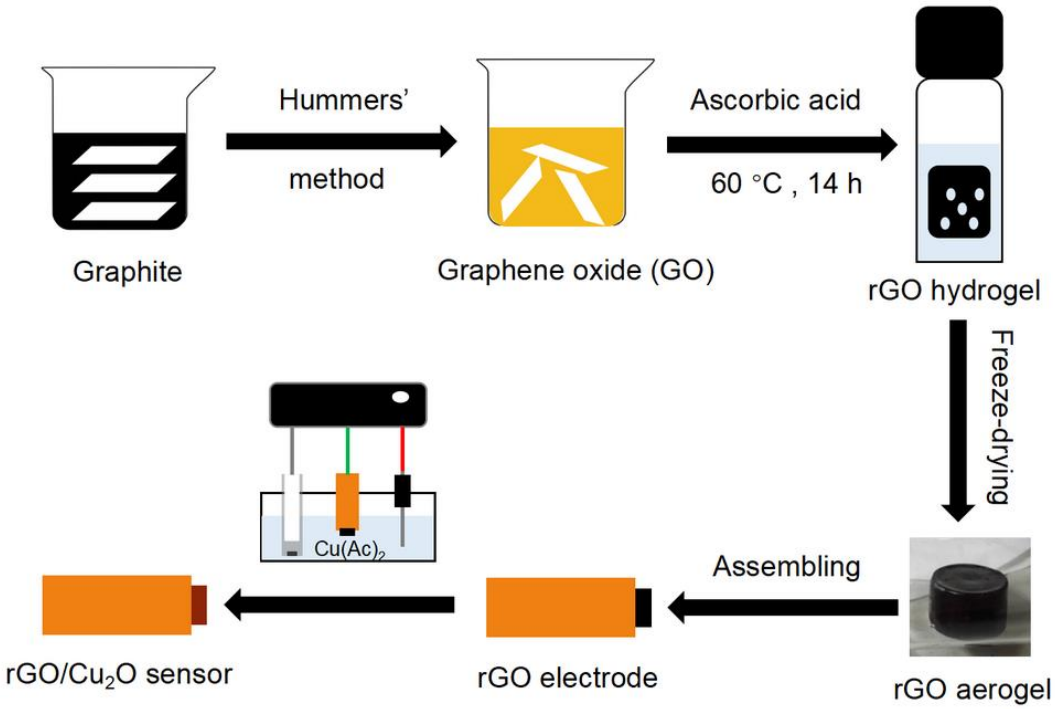

Scheme 1. Schematic of the preparation procedure of an rGO/Cu_2O sensor.

The morphologies of the materials were observed by a Hitachi SU8010 scanning electron microscope (SEM), and the X-ray diffraction (XRD) patterns were investigated by a Shimadzu XRD-7000. X-ray photoelectron spectroscopic (XPS) data were obtained from the Kratos AXIS Ultra at Al-Kα radiation. Raman spectra were obtained on a Horiba XploRA confocal microscope upon 532-nm laser excitation. The electrochemical tests were carried out on the CHI-660 electrochemical work station (Chenhua, Shanghai).

3. RESULTS AND DISCUSSION

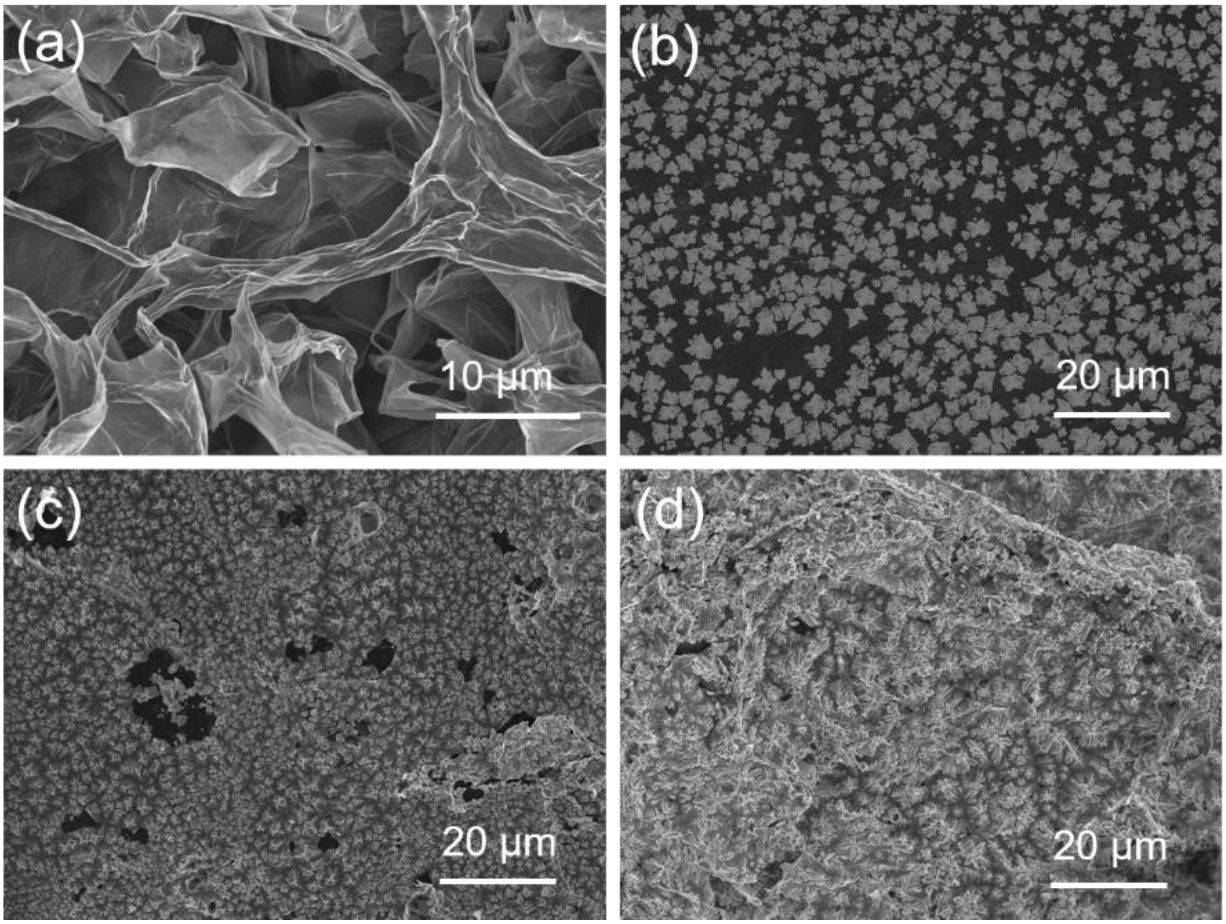

Figure 1. SEM images of (a) an rGO aerogel and rGO/Cu_2O samples with different Cu_2O electrodeposition times of (b) 2 min, (c) 8 min and (d) 16 min.

Compared with the conventional chemical synthesis method or physical adsorption approach for graphene-Cu_2O composite fabrication, electrodeposition is simpler, more environmentally friendly and easier to control. The morphology of the pristine rGO aerogel and the aerogel decorated with Cu_2O after different electrodeposition times were characterized by SEM. Figure 1a clearly shows that the rGO aerogel exhibits a porous structure from the interconnected graphene sheets. After 2 min of electrodeposition, as shown in Figure 1b, the star-like Cu_2O crystalline particles of approximate 5 μm are homogeneously distributed on the surface of the rGO film (rGO/Cu_2O-2). With an increase in the electrodeposition time to 8 min (rGO/Cu_2O-8), the Cu_2O crystals become much denser and cover most of the rGO surface (Figure 1c). When the electrodeposition time reaches 16 min (rGO/Cu_2O-16), the surface of the film is almost fully covered by Cu_2O particles (Figure 1d), which impedes the conduction between rGO and the tested solution in the electrochemical measurement and leads to inferior sensing performance.

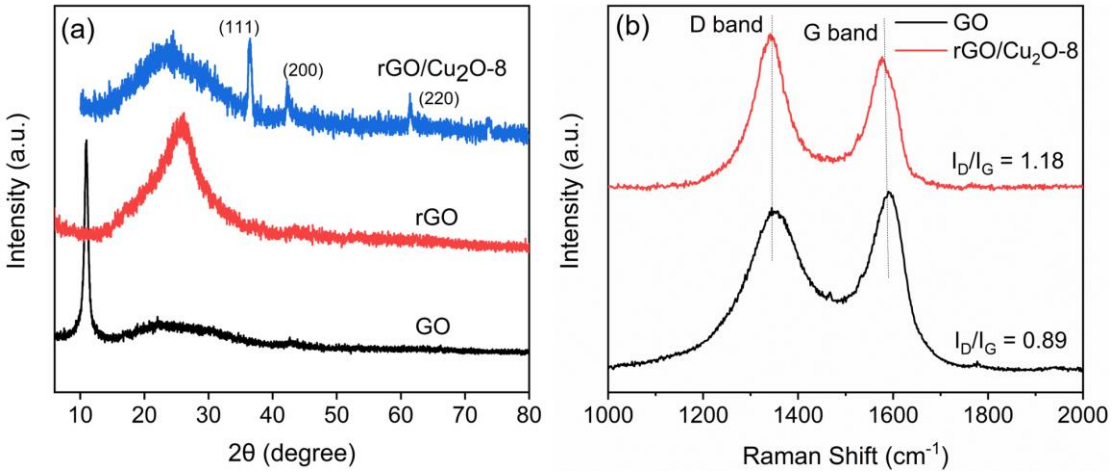

Figure 2. (a) XRD patterns of the GO, rGO and Cu_2O/rGO-8 samples. (b) Raman spectra of the GO and rGO/Cu_2O-8 samples.

To further analyze the structure of the samples, XRD and Raman characterizations were conducted. As displayed in Figure 2a, for pristine GO and rGO, the XRD peaks at 11.2° and 25.4°, respectively, indicate that the GO was reduced by the hydrothermal method. For the Cu_2O/rGO-8 sample, four strong diffraction peaks with 2θ values of 36.5°, 42.4°, 61.5° and 73.7° are clearly observed, which is in accordance with the standard data of Cu_2O (JCPDS file No. 05-0667) [31]. The Raman spectra of the prepared GO and rGO/Cu_2O-8 are shown in Figure 2b, both of which exhibit the D band at 1335 cm^{-1} and the G band 1580 cm^{-1}, which are attributed to the sp^2 and sp^3 carbons of graphene, respectively. Moreover, the rGO/Cu_2O-8 sample presents an I_D/I_G (the intensity ratio of the D band to the G band) value of 1.18, which is higher than the value of 0.89 for GO, indicating an increase in carbon disorder for the former, probably because of the decrease in the graphene sheet size upon reduction [32].

The detailed element information of the composite could be obtained from the XPS analysis. As shown in Figure 3a, the entire XPS spectrum of the Cu_2O/rGO-8 sample demonstrates the featured signals of Cu 2p, C 1s and O 1s with the respective binding energy of 940, 285 and 532 eV. The deconvoluted C 1s spectra for is depicted in Figure 3b, in which the peaks located at 284.5, 285.8, 287.7 and 288.6 eV are ascribed to C=C, C-OH, C=O and O-C=O of rGO, respectively [33]. The deconvoluted Cu 2p spectrum shown in Figure 3c displays the peaks at 932.4 and 952.0 eV, assigned to the Cu $2p_{3/2}$ and Cu $2p_{1/2}$ of Cu^+, respectively. Meanwhile, the peaks at 934.3 and 954.2 eV should come from $CuO/Cu(OH)_2$, owning to oxidation of Cu^+ under the ordinary experimental condition.

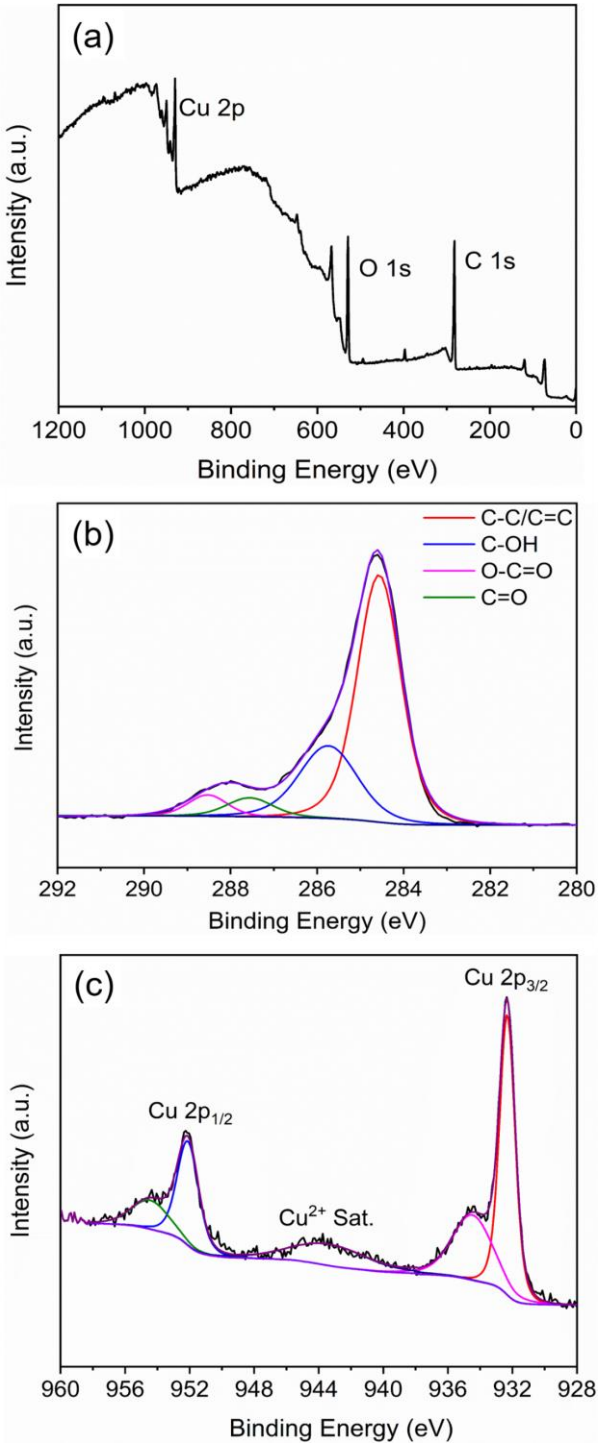

Figure 3. (a) XPS spectra of the Cu_2O/rGO-8 sample and deconvoluted (b) C 1s and (c) Cu 2p XPS peaks of the sample.

The electrocatalytic performance of the rGO/Cu_2O film electrode toward H_2O_2 was examined through cyclic voltammetry (CV) measurements. Figure 4a presents the CV curves of the rGO/Cu_2O-8 electrode in phosphate buffer solution (PBS, pH = 7.0) with/without H_2O_2. Obviously, compared with

the response to the bare PBS, the CV curve exhibits a larger background current toward 0.1 mM H_2O_2 with the enhanced reduction current centered at –0.15 V, indicating the good electrocatalytic effect of the electrode on the reduction of H_2O_2. The influence of different Cu_2O electrodeposition times on the electrochemical performance of rGO/Cu_2O electrodes is displayed in Figure 4b. It is clearly seen that, compared with the rGO/Cu_2O electrodes, the rGO electrode presents inferior performance owing to the absence of Cu_2O. The rGO/Cu_2O-2 electrode displays a remarkable current enhancement, which is ascribed to the excellent catalytic ability of Cu_2O and the synergistic effect with the porous rGO substrate [34]. With more Cu_2O deposition, the rGO/Cu_2O-8 electrode exhibits a higher peak current than the rGO/Cu_2O-2 electrode, suggesting a better Cu_2O deposition amount for the electrocatalytic performance of the composite electrode. However, as the electrodeposition time reaches 16 min, the resulting rGO/Cu_2O-16 electrode yields a decreasing current, which should be attributed to an increase in the electrode resistance owing to the overcovering of rGO sheets with Cu_2O, consistent with the SEM characterization (Figure 1d). Hence, 8 min is the optimal electrodeposition time, and the rGO/Cu_2O-8 sample is chosen for the following experiments.

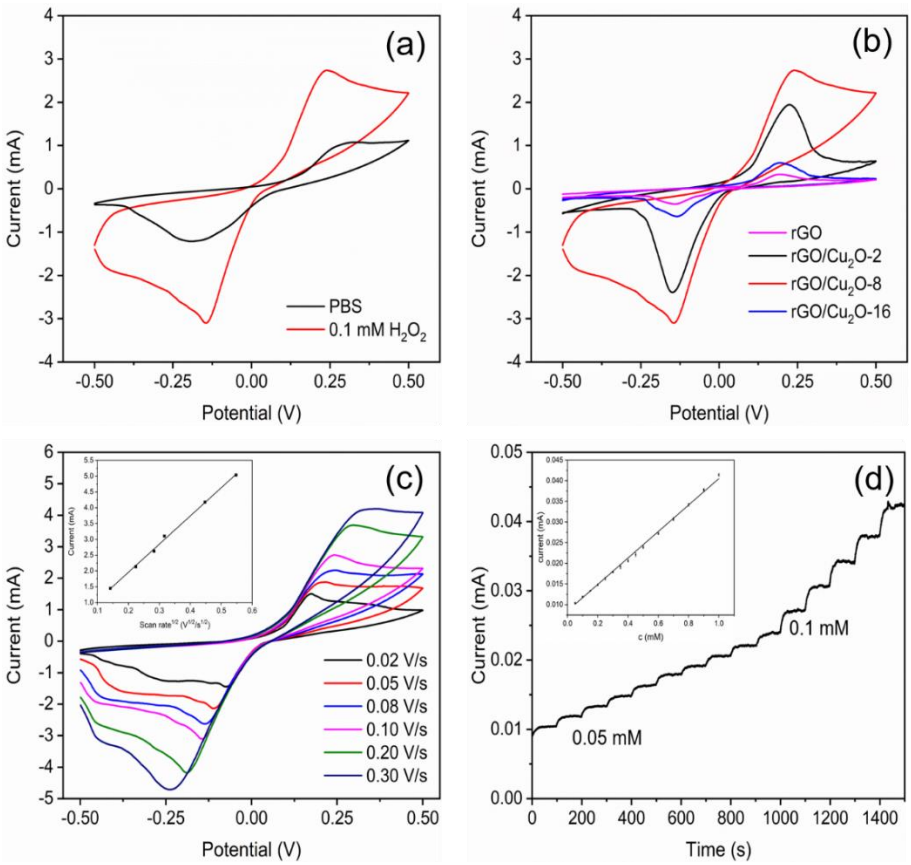

Figure 4. (a) CV curves of the rGO/Cu_2O-8 electrode in PBS with and without 0.1 mM H_2O_2. (b) CV curves of different rGO/Cu_2O electrodes in 0.1 mM H_2O_2. (c) CV curves of the rGO/Cu_2O-8 electrode in 0.1 mM H_2O_2 at various scan rates. The inset depicts the relationship between the reduction currents and the square roots of the scan rates. (d) Responses of the rGO/Cu_2O-8 electrode with H_2O_2 addition of H_2O_2 at – 0.2 V, and the inset depicts the current increase tendency along with the H_2O_2 concentration. All the measurements were obtained in 0.1 M PBS (pH = 7.0).

The CV performances of the Cu_2O/rGO-8 electrode in 0.1 mM H_2O_2 at various scan rates were investigated, and the CV curves are shown in Figure 4c. Obviously, as the scan rate increases from 0.02 V/s to 0.30 V/s, the peak current increases gradually. The inset in Figure 4c reveals the linear dependence of the reduction current on the square root of the scan rate, indicating that the electron transport is ascribed to the diffusion-controlled process. The current-time plot in Figure 4d shows the increase in the current of the rGO/Cu_2O-8 sensor upon injection of 0.05 mM (0 to 1000 s) and 0.1 mM (1000 to 1500 s) H_2O_2 into the stirring PBS. We can see that the reduction current responds quickly upon each addition of H_2O_2 and exhibits a regular stepwise increase accompanied by a consecutive increase in H_2O_2 concentration. The inset shows the linear relation between the current and the concentration, with a satisfactory scale from 0.05 to 1.1 mM (R^2 = 0.9998). Finally, with a signal/noise value of 3, a limit of detection (LOD) of 12 μM could be determined, implying good sensitivity for the hydrogel sensor. The electrochemical sensing capacity toward H_2O_2 of the Cu_2O/rGO-8 hydrogel electrode is also compared with those of some typical Cu_2O-based sensors in the literature, as displayed in Table 1. Most of the sensors are Cu_2O-modified GCEs, and the rest are based on conductive substrates. The freestanding Cu_2O/rGO-8 hydrogel electrode in this work exhibits a performance comparable to that of the other reported sensors in terms of the parameters of linear range or LOD value.

Table 1. Comparison of the H_2O_2 detection performance of reported electrochemical Cu_2O-based sensors and the sensor reported in this work.

Electrode material	Potential (V)	Linear range (mM)	LOD (μM)	Ref
Graphene/Cu_2O-GCE	-0.4 (*vs* Ag/AgCl)	0.3-7.8	20.8	18
2D-Cu_2O-rGO-GCE	-0.4 (*vs* Ag/AgCl)	0.005-10.56	3.78	20
Cu_2O/graphene-stainless steel	-0.2 (*vs* Ag/AgCl)	0.002-1.057	0.34	25
Cu_2O-rGO-GCE	-0.2 (*vs* Ag/AgCl)	0.1-9.8	79.0	34
Cubic-Cu_2O-GCE	-0.2 (*vs.* Ag/AgCl)	0.05-3.4	12.4	35
Cu_2O/TiO_2-Ti foil	-0.4 (*vs*. Hg/Hg_2Cl_2)	0.5-8	90.5	36
Pt-Cu_2O/Nafion-GCE	-0.25 (*vs.* Ag/AgCl)	0.01-6	10.3	37
rGO/Cu_2O hydrogel	-0.2 *vs.* (Ag/AgCl)	0.05-1.1	12.0	This work

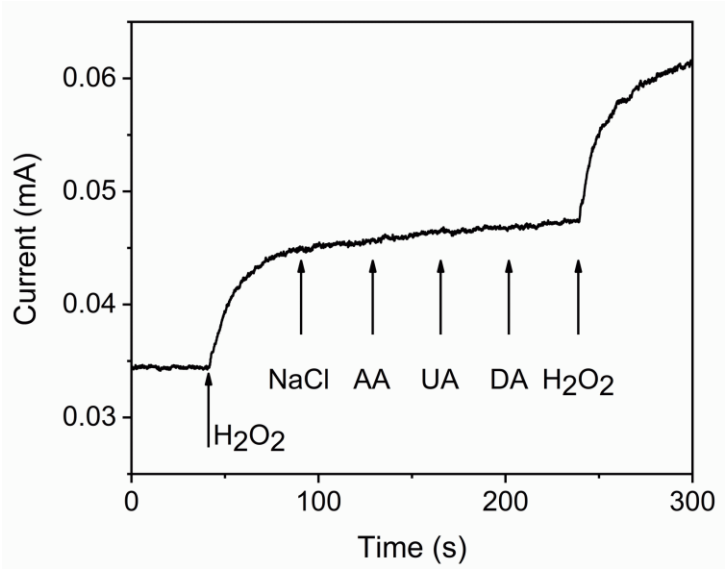

Figure 5. The current response of the Cu_2O/rGO-8 electrode for H_2O_2 upon the addition of NaCl, ascorbic acid (AA), uric acid (UA) and dopamine (DA).

To evaluate the anti-interference ability of the rGO/Cu_2O-8 electrode against some possible impurities, such as NaCl, ascorbic acid, uric acid and dopamine, the steady-state amperometric response of the electrode in H_2O_2 measurement was tested with the respective addition of the substances mentioned above. The results shown in Figure 5 demonstrate that these interfering substances do not cause an obvious change in the current, and the final H_2O_2 addition increases the current response, suggesting that the sensor has good selectivity in sensing H_2O_2.

4. CONCLUSIONS

We have developed a convenient and cost-efficient method for fabricating Cu_2O-graphene composite films that can be directly utilized as electrochemical H_2O_2 sensors. The graphene hydrogel could be obtained through a mild hydrothermal process, and the corresponding hydrogel film could serve as the freestanding substrate electrode for controllable electrodeposition of Cu_2O. The as-prepared hydrogel composites were characterized by SEM, XRD, Raman and XPS. The electrochemical measurements demonstrate the optimal electrodeposition time of 8 min, which yields the rGO/Cu_2O-8 electrode for electrocatalytic reduction of H_2O_2. The rGO/Cu_2O hydrogel film electrode exhibits good sensing performance for H_2O_2 detection, including high sensitivity, fast response, low detection limit and good selectivity. Our report could help to explore unconventional sensors/biosensors from hydrogel materials.

ACKNOWLEDGEMENT
This work was supported by the National Natural Science Foundation of China (Grant No. 21973112) and the Fundamental Research Funds for the Central Universities, the Research Funds of Renmin University of China (Grant No. 16XNLQ04).

References

1. K. S. Novoselov, V. I. Fal'ko, L.Colombo, P. R. Gellert, M. G. Schwab and K. Kim, *Nature*, 490 (2012) 192.
2. Y. Zhu, S. Murali, W. Cai, X. Li, J. W. Suk, J. R. Potts and R. S. Ruoff, *Adv. Mater*., 22 (2010) 3906.
3. S. J. Guo and S. J. Dong, *Chem. Soc. Rev*., 40 (2011) 2644.
4. D. Y. Zheng, H. Hu, X. J. Liu and S. S. Hu, *Curr. Opin. Colloid Interface Sci*, 20 (2015) 383.
5. M. Coros, S. Pruneanu and Staden, RI. Stefan-van, *J. Electrochem. Soc*., 167 (2019) 037528.
6. W. Chen, S. Cai, Q. Q. Ren, W. Wen and Y. D. Zhao, *Analyst,* 137 (2012) 49.
7. J. S. Kumar, N. C. Murmu and T. Kuila, *AIMS Mater. Sci.,* 5 (2018) 422.
8. X. B. Lu, Q. Zhang, L. Zhang and J. H. Li, *Electrochem. Commun*., 8 (2006) 874.
9. H. Shamkhalichenar and J. W. Choi, *J. Electrochem. Soc*., 167 (2020) 037531.
10. R. Z. Zhang and W. Chen, *Biosens. Bioelectron*., 89 (2017) 249.
11. F. Xiao, J. B. Song, H. C. Gao, X. L. Zan, R. Xu and H. W. Duan, *ACS Nano*, 6 (2012) 100.
12. Z. M. Ma, B. Y. Wang, K. Y. Cui, Y. Wang and S. J. Li, *Int. J. Electrochem. Sci*., 14 (2019) 6840.
13. Y. M. Sun, K. He, Z. F. Zhang, A. J. Zhou and H. W. Duan, *Biosens. Bioelectron*., 68 (2015) 358.
14. Q. Xi, X. Chen, D. G. Evans and W. S. Yang, *Langmuir*, 28 (2012) 9885.
15. H. Zhu, L. Li, W. Zhou, Z. P. Shao and X. J. Chen, *J. Mat. Chem*. B, 4 (2016) 7333.
16. L. J. Kong, Z. Y. Ren, N. N. Zheng, S. C. Du, J. Wu, J. L. Tang and H. G. Fu, *Nano Res*., 8 (2015) 469.
17. S. J. He, B. Y. Zhang, M. M. Liu and W. Chen, *RSC Adv*., 4 (2014) 49315.
18. M. M. Liu, R. Liu and W. Chen, *Biosens. Bioelectron*., 45 (2013) 206.
19. S. D. Sun, X. J. Zhang, Q. Yang, S. H. Liang, X. Z. Zhang and Z. M. Yang, *Prog. Mater. Sci*., 96 (2018) 111.
20. C. F. Cheng, C. M. Zhang, X. H. Gao, Z. H. Zhuang, C. Du and W. Chen, *Anal. Chem*., 90 (2018) 1983.
21. C. Janaky, E. Kecsenovity and K Rajeshwar, *ChemElectroChem*, 3 (2016) 181.
22. S. X. Wu, Z. Y. Yin, Q. Y. He, X. A. Huang, X. Z. Zhou and H. Zhang, *J. Phys. Chem*. C, 114 (2010) 11816.
23. Y. X. Zhou, L. P. Jia, T. X. Wang, Y. L. Du and C. M. Wang, *Int. J. Hydrog. Energy*, 43 (2018) 7356.
24. B. Q. Yuan, C. Y. Xu, L. Liu, Q. Q. Zhang, S. Q. Ji, L. P. Pi, D. J. Zhang, Q. S. Huo, *Electrochim. Acta*, 104 (2013) 78.
25. J. S. Kumar, N. C. Murmu, P. Samanta and T. Kuila, *New J. Chem*., 42 (2018) 3574.
26. J. F. Zeng, X. T. Ding, L. W. Chen, L. Jiao, Y. Z. Wang, C. D. Windle, Q. Han, L. and T. Qu, *RSC Adv*., 9 (2019) 28207.
27. Z. Li, Z. Liu, H. Y. Sun, and C. Gao, *Chem. Rev*., 115 (2015) 7046.
28. M. H. Yu, W. T. Qiu, F. X. Wang, T. Zhai, P. P. Fang, X. H. Lu and Y. X. Tong, *J. Mater. Chem*. A, 3 (2015) 15792.
29. Z. Y. Sui, Y. Cui, J. H. Zhu and B. H. Han, *ACS Appl. Mater. Interfaces*, 5 (2013) 9172.
30. F. Sun and Z. Wang, *Mater. Lett*. 234 (2019) 62.
31. J. S. Kumar, N. C. Murmu, P. Samanta and T. Kuila, *New J. Chem*., 42 (2018) 3574.
32. S. Mutyala and J. Mathiyarasu, *Mater. Sci. Eng. C-Mater. Biol. Appl*., 69 (2016) 398.

33. O. C. Compton, D. A. Dikin, K. W. Putz, L. C. Brinson and S. T. Nguyen, *Adv. Mater*., 22(2010) 892.
34. F. G. Xu, M. Deng, G. Y. Li, S. H. Chen and L. Wang, *Electrochim. Acta*, 88 (2013) 59.
35. Y. M. Zhong, Y. C. Li, S. X. Li, S. Q. Feng, and Y. Y. Zhang, *RSC Adv*., 4 (2014) 40638.
36. X. Wen, M. Long, and A. D. Tang, *J. Electroanal. Chem*., 785 (2017) 33.
37. J. Lv, C. C. Kong, K. Liu, L. Yin, B. Ma, X. J. Zhang, S. Yang and Z. M. Yang, *Chem. Commun*., 54 (2018) 8458.